Computing elastic anisotropy to discover gum-metal-like structural alloys

I. S. Winter, M. de Jong, M. Asta, and D. C. Chrzan

Phys. Rev. Materials **1**, 030601 — Published 11 August 2017

DOI: 10.1103/PhysRevMaterials.1.030601

Computing elastic anisotropy to discover Gum-Metal-like structural alloys

I. S. Winter,[1,2] M. de Jong,[1] M. Asta,[1,3] and D. C. Chrzan[1,3,*]

[1]*Department of Materials Science and Engineering, University of California, Berkeley, California 94720, USA*

[2]*Energy Technologies Area Division, Lawrence Berkeley National Laboratory, Berkeley, California, 94720, USA*

[3]*Materials Sciences Division, Lawrence Berkeley National Laboratory, Berkeley, California, 94720, USA*

Abstract

The computer aided discovery of structural alloys is a burgeoning but still challenging area of research. A primary challenge in the field is to identify computable screening parameters that embody key structural alloy properties. Here, an elastic anisotropy parameter that captures a material's susceptibility to solute solution strengthening is identified. The parameter has many applications in the discovery and optimization of structural materials. As a first example, the parameter is used to identify alloys that might display the super elasticity, super strength and high ductility of the class of TiNb alloys known as Gum Metals. In addition, it is noted that the parameter can be used to screen candidate alloys for shape memory response, and potentially aid in the optimization of the mechanical properties of high entropy alloys.

The computer-aided design of structural alloys is, by now, a well established field [1–4]. Most often, computation is used to improve the properties of an existing structural material (e.g. steel, Ti, Al-alloys), and improvements are based on the fundamental understanding of the deformation mechanisms governing the mechanical properties of the alloys (e.g. dislocation slip vs. twinning). While the insights obtained are impressive and technologically important, they ultimately lead to improvements in relatively well-understood structural materials with well-understood deformation mechanisms.

In contrast, the computational discovery of structural materials is far less common. Typically, the search has focused on identifying super-hard materials [5–9], as one can screen for these materials by evaluating combinations of the elastic constants. While super-hard materials find structural applications, the broader class of structural alloys includes those that can be plastically deformed more extensively. To address this need, recent efforts focus on the discovery of high entropy alloys (HEAs) [10–12] with the goal of increasing the stability of a given phase, but not necessarily optimizing mechanical properties. Li *et al.* [13] note that dual phase HEA alloys can be made very strong *and* tough. The mechanisms invoked to explain this effect are the extreme solid solution strengthening observed in HEAs and a phase transformation induced hardening of the second phase. Notably, the improvement in mechanical properties is achieved by *reducing* the stability of the relevant phases.

In 2003, researchers at Toyota introduced a Ti-Nb based alloy named Gum Metal [14]. This body-centered-cubic (BCC) solid solution alloy displays numerous technologically interesting properties, many of which emerge only after extensive cold-working of the material. These properties include super-elasticity (an elastic limit of approximately 2.5% at room temperature), a near constant Young's modulus and zero thermal expansion coefficient from about 80 K - 550 K, little or no work-hardening while still displaying over 12% elongation, and a high yield strength (~1.2 GPa). Surprisingly, post mortem microstructural investigations revealed a dearth of dislocations [14]. This fact, coupled with the observation that the strength of Gum Metal is comparable to its ideal shear strength (ISS), led Saito *et al.* to conclude that Gum Metal is a bulk engineering alloy that deforms at ideal strength.

This claim remains controversial as it seems to contradict 80 years of metallurgical wisdom asserting that bulk alloys do not deform at ISS. Accordingly, the deformation of Gum Metal has attracted much attention, and the deformation mechanisms leading to its unusual behavior are beginning to be identified [15–19].

Since the 1970's certain TiNb alloys have been known to behave as shape memory alloys (SMAs) [20]. Gum Metal was developed by tuning the composition of a TiNb alloy (similar to that of SMAs) near instability (driving its shear modulus $C' = \frac{1}{2}(C_{11} - C_{12})$) to zero, placing the alloy near the β (BCC) to α (hexagonal-close-packed; HCP) transus [14, 21, 22]. The same approach was applied to develop another Gum-Metal-like alloy that exploits proximity to the face-centered-cubic (FCC) to BCC transition. This Fe-Ni-Co-Ti alloy is ductile (elongation to fracture of 9.4%) while having a yield strength of 2.2 GPa [23]. So known Gum Metals are similar to the tough, ductile HEAs [13] in that they, too, have been engineered to be near the limits of structural stability.

Theoretical work suggests that Gum-Metal-like behavior is possible near other phase transitions as well [24]. The form of the elastic anisotropy that develops at the transitions between BCC, FCC and HCP phases can spread the dislocation cores [24, 25] and make the dislocations extremely susceptible to pinning by obstacles (and consequently extremely susceptible to solid solution strengthening), even at stresses approaching ISS [15]. Moreover, the spreading and overlap of dislocation cores can lead to the appearance of nanodisturbances in the microstructure [25, 26], a defect structure observed in Gum Metal. Interestingly, all of these properties can be deduced from a simple calculation of the elastic constants of the materials, and from computation of their ideal strengths [15, 24, 25, 27–30]. So, while the deformation mechanism active in Gum Metal remains controversial, the materials properties that lead to Gum-Metal-like behavior can be identified.

This observation enables a purely computational approach to the discovery of Gum-Metal-like alloys: (1) Develop a general elastic anisotropy parameter, A_c, that is related to the susceptibility of a dislocation to being pinned and can be used to construct a structure map. (2) Evaluate this parameter for a set of materials. (3) Screen for materials of especially high anisotropy A_c. (4) Assess the elastic stability of solid solution alloys with the same composition.

Using the Materials Project's elastic constants database [31, 32], we consider the materials in space groups 225 and 229, and identify alloys with the propensity to display Gum-Metal-like behavior. Many of the identified alloys are known shape memory alloys. Of these, alloys based on the Al-Cu or Al-Cu-Mn system seem most promising technologically and are explored in more detail. We further suggest that our parameter, A_c, can be used to identify materials that are highly susceptible to solid solution strengthening, perhaps aiding in the

design of HEAs.

The means by which elastic anisotropy impacts dislocation core structures leads to a suitable definition of A_c. A requirement for a material to fail at its ideal strength is that the stress needed to initiate dislocation motion must be greater than ISS. This stress can be estimated using a simple two-dimensional line tension model that looks at the interaction of a dislocation with a random array of infinitesimal pinning sites [33]. The critical shear stress for dislocation motion in this model scales inversely with the average distance between pinning sites and scales linearly with the dislocation energy factor.

By equating the critical shear stress for dislocation motion to ISS, the critical non-dimensional average pinning length of obstacles, $l_c^* = l/b$ can be determined [15]. For many systems, it is reasonable to assume that ISS scales with a particular shear modulus, $G_{\{hkl\}\langle uvw\rangle}$. Taking as an example the case of a $\langle 111\rangle$ type screw dislocation in BCC, the ISS can be approximated as $\sigma_{ideal} = 0.11 G_{\langle 111\rangle}$ (the shear modulus along $\langle 111\rangle$ is isotropic with respect to the shear plane for BCC) [34]. The modulus governing the dislocation line tension can be determined analytically in terms of the elastic constants. This results in

$$l_c^* \propto \frac{K_s}{G_{111}} = \sqrt{\frac{(C_{11}-C_{12}+4C_{44})(2C_{11}^2+2C_{11}C_{12}-4C_{12}^2+13C_{11}C_{44}-7C_{12}C_{44}+2C_{44}^2)}{27C_{44}(C_{11}-C_{12})(C_{11}+C_{12}+2C_{44})}}. \tag{1}$$

The ratio $K_s/G_{\langle 111\rangle}$ can be viewed as an anisotropy parameter (in an isotropic material, the ratio is one). For screw dislocations in BCC crystals, the ratio is inversely proportional to $\sqrt{C_{11}-C_{12}}$ and $\sqrt{C_{44}}$. As an elastic instability is approached and these shear moduli approach 0, $K_s/G_{\langle 111\rangle} \to \infty$, and l_c^* diverges. Similar behavior is found to accompany the elastic instability of edge dislocations in BCC [15] and for dislocations in materials near other phase transitions [24]. Materials with large values of the anisotropy parameter $\frac{K}{G}$ have the potential to display Gum-Metal-like behavior.

An elastic anisotropy parameter for any crystalline system can be derived from Stroh's formalism [35]. Accordingly, the general non-dimensional elastic anisotropy parameter related to the pinning of dislocations is defined as

$$A_c = \frac{b_p K_{pq} b_q}{b^2 G_{min}}, \tag{2}$$

where G_{min} is the smallest shear modulus oriented along the Burgers vector ($\boldsymbol{b}$, components b_p), $\boldsymbol{K}$ (with components K_{pq}) is the modulus associated with the energy factor of a dislocation and the Einstein summation convention is assumed. (For details on the calculation of $\boldsymbol{K}$ see the supplementary materials.) A_c can be evaluated for hundreds of compounds in a matter of minutes. One can then construct an A_c-based structure map by plotting the points $\left(A_c^{screw}, A_c^{edge}\right)$ for each of the considered materials, with $A_c^{screw}(A_c^{edge})$ the computed anisotropy for screw(edge) dislocations with a given $\boldsymbol{b}$.

To construct the structure map, A_c was computed for all materials in the Materials Project [31] elastic constants database with symmetry spacegroups $Im\bar{3}m$ (229) and $Fm\bar{3}m$ (225). Spacegroup 229 contains BCC while spacegroup 225 encompasses FCC as well as ordered structures with atomic positions consistent with BCC such as $D0_3$ and $L2_1$. Calculations of A_c were carried out for both screw and edge dislocations with $\boldsymbol{b}$ in the direction $\langle 111\rangle$ and $\langle 110\rangle$. In the case of edge dislocations the slip systems used were $\langle 111\rangle\{1\bar{1}0\}$ and $\langle 110\rangle\{1\bar{1}1\}$.

The structure maps for compounds in space group 225 are shown in FIG. 1. (The structure maps for space group 229 are presented in the supplemental materials. They reveal similar trends.) The structure maps clearly separate the materials by anisotropy. Moreover, approximately the same ordering of materials by anisotropy is seen regardless of slip direction. For instance, in the case of the space group 225 compounds the Spearman rank correlation coefficient between the two slip directions is 0.998 and 0.790 for a screw and edge dislocation respectively.

The structure maps reveal interesting trends. First, consider the Ti-Nb and Ti-V approximants to Gum Metal plotted in FIGs. 1 and 2. When viewed on the structure map, the Ti-Nb approximants to Gum Metal do not have the most extreme A_c's of the compounds plotted. However, Gum Metal itself is a much more complicated alloy than the approximants and can include significant additions of O, Hf, Ta, Zr and V. The Ti-V approximants to Gum Metal, as computed using the virtual crystal approximation, reveal that the anisotropy ratios can be very sensitive to the number of valence electrons. Near the point of instability, a 10% change in valence electron count leads to almost a factor of two change in A_c^{edge}. So it is possible that while Ti-Nb does not itself possess an extreme A_c, the effects of alloying additions may lead to a substantially larger A_c than computed here. Importantly, the map reveals that there are stoichiometric intermetallic compounds that have larger A_c's than the

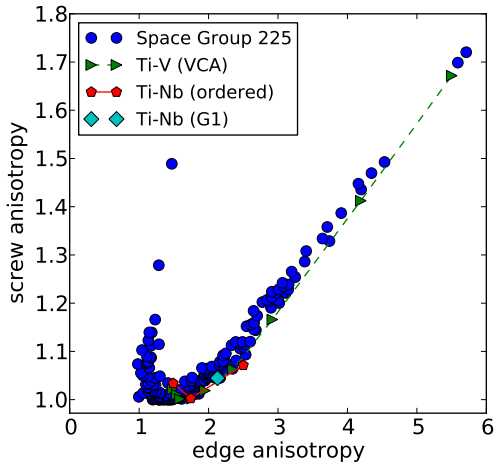

a)

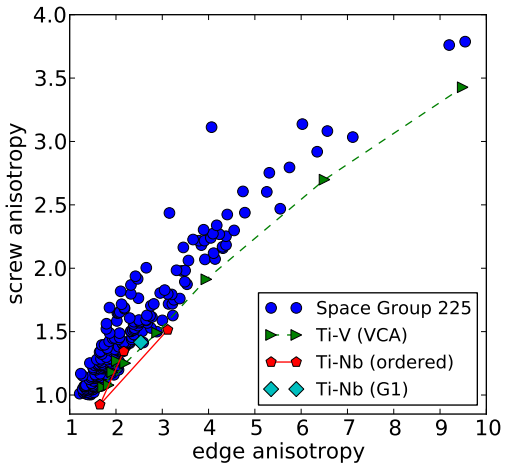

b)

FIG. 1. Comparison of the anisotropy parameter of the 227 materials with space group 225 with selected Ti-Nb and Ti-V systems for both an edge and screw dislocation for Burgers vectors oriented in the $\langle 111 \rangle$ and $\langle 110 \rangle$ directions. The Ti-Nb ordered systems consist of 25, 50, and 75 at. % Ti[22]. The VCA calculation consists of nine compositions at 5, 15, 25, 35, 45, 55, 65, 75, and 80 % Ti system[15, 25]. The G1 structure is known to be the lowest energy 16 atom configuration for 25 at. % Ti as calculated in DFT[36].

prototypical alloy. These are the compounds of interest.

The structure maps also show a noticeable branching in the data, especially at higher screw dislocation anisotropies. At high anisotropy for slip in the $\langle 110 \rangle$ direction, the left branch appears almost linear and the right branch trends sublinear with increasing edge

anisotropy. For $\langle 110\rangle\{001\}$ slip, an analytical solution is available for both edge and screw dislocations. This solution indicates that the branches develop because of two different types of instability: $C_{44} \to 0$ and $C_{11} - C_{12} \to 0$ (see supplementary materials). Further examination of the numerical results in FIG. 1 reveal that the branching has the same origins. Hence, the structure map is able to separate compounds according to the type of instability.

TABLE I. Listing of the compounds from spacegroup 225 that contained the highest screw anisotropy.

Compound	$A_c^{screw}(\langle 110\rangle)$	$A_c^{edge}(\langle 110\rangle\{111\})$	$A_c^{screw}(\langle 111\rangle)$	$A_c^{edge}(\langle 111\rangle\{110\})$	lowest shear modulus
$LiSiCu_2$	2.42	4.18	1.27	3.20	C'
ZrS	2.44	3.15	1.28	1.28	C_{44}
YCd_3	2.44	4.78	1.29	3.38	C'
$TiAlPd_2$	2.47	5.55	1.33	3.74	C'
$MgCdAg_2$	2.60	5.26	1.33	3.64	C'
Li_3In	2.60	4.74	1.31	3.41	C'
Li_2MgCd	2.75	5.31	1.36	3.71	C'
$AlCu_3$	2.79	5.75	1.39	3.91	C'
$LiAg_2Ge$	2.92	6.35	1.44	4.20	C'
$MnAlPd_2$	3.03	7.11	1.49	4.53	C'
$MnAlCu_2$	3.08	6.57	1.47	4.34	C'
YTe	3.11	4.07	1.48	1.47	C_{44}
Li_2ZnSn	3.14	6.03	1.45	4.16	C'
Li_3Pd	3.76	9.20	1.70	5.59	C'

In Table I the compounds in spacegroup 225 ($Fm\bar{3}m$) with the highest values of A_c^{screw} are listed (a table of all compounds is included in the supplementary materials). This table reveals interesting trends. Many of the compounds contain Li or Pd. For reference, Li has the highest A_c values of all BCC materials with $A_c^{screw}(\boldsymbol{b} = \langle 111\rangle) = 1.61$ and $A_c^{screw}(\boldsymbol{b} = \langle 110\rangle) = 3.47$. Another observation is that alloys of similar compositions to the compounds shown in Table I are known to be SMAs. It is already known that many SMAs have a low value of C'[21, 37, 38]. Al-Cu-Mn systems are known SMAs[39]. TiPd

(similar to $TiAlPd_2$) has been shown to be a high-temperature SMA[40, 41]. The emergence of the shape memory effect appears to accompany higher anisotropy in the Ti-Nb and Ti-V systems as well. For instance, Ti-(22-27) at.% Nb alloys and Ti-10V-2Fe-3Al (83.8 at.% Ti)[42] exhibit shape memory behavior[20, 38].

Two of the compounds in the table were selected for further study: $AlCu_3$ and $MnAlCu_2$. These compounds were selected because they contain relatively inexpensive materials, and if alloys with Gum-Metal-like properties can be formed at or near these compositions, they are likely to have a significant technological impact. Since Gum-Metal-like behavior emerges in the disordered solid solution phase, it is interesting to explore if solid solutions at these compositions remain elastically stable.

Elastic constants were computed using density functional theory (DFT) as implemented in the Vienna Ab initio Simulation Package (VASP) [43, 44]. The Perdew, Becke, and Ernzerhof (PBE) Generalized Gradient Approximation exchange-correlation functional was employed [45]. A plane-wave cutoff of 400 eV was used with a first-order Methfessel-Paxton smearing[46] employing a smearing parameter of 0.05 eV. Ionic relaxations were performed until all forces were less than 0.005 eV/Å. A $15 \times 15 \times 15$ Γ-centered k-point mesh was employed, which ensured that the elastic constants were converged to less than a 2% difference for $MnAlCu_2$ and a 10% difference for $AlCu_3$. To approximate a solid solution a 16-atom special quasirandom structure (SQS) [47, 48] was generated using the alloy theoretic automated toolkit (ATAT) [49]. Both pairs and triplet clusters were considered within a range of $3a_0$, a_0 being the lattice parameter associated with the (on average) BCC crystal. The elastic constants were calculated performing 4 deformations of varying magnitude for the six independent strains and after obtaining the stresses from VASP performing a linear fit [50]. The elastic constants were then symmetrized by generating the 48 transformation matrices associated with the point group of a BCC crystal and then averaging the elastic constants over the transformations

$$C_{ijkl}^{sym} = \frac{1}{48} \sum_{\alpha=1}^{48} a_{ip}^{(\alpha)} a_{jq}^{(\alpha)} a_{kr}^{(\alpha)} a_{ls}^{(\alpha)} C_{pqrs}, \tag{3}$$

with $\boldsymbol{a}^{(\alpha)}$ corresponding to the transformation matrix of the α^{th} element of the point group. For $MnAlCu_2$ the unit cell was initialized in a ferromagnetic state.

Our calculations for the $AlCu_3$ ($D0_3$) and $MnAlCu_2$ ($L2_1$) ordered structures broadly

match those generated by the materials project (see Table II). For the $AlCu_3$ phase, there is a 9% difference in the values of C_{44}, which is relatively large, but not atypical for DFT calculations of the elastic constants. The $AlCu_3$ SQS structure also has noticeably different elastic constants compared to the ordered structure, with the disordered phase being elastically unstable ($C_{11} - C_{12} < 0$). This is not surprising considering that the ordered structure is already highly elastically anisotropic, and for such materials, changes in ordering can drastically change the elastic behavior [36].

TABLE II. Calculated SOEC's from DFT for ordered and disordered structures of Al-Cu system as well as ordered $MnAlCu_2$. C_{11}, C_{12}, and C_{44} are all in GPa.

Compound	$AlCu_3$ ($D0_3$)[32]	$AlCu_3$ ($D0_3$)	$Al_{0.25}Cu_{0.75}$ (SQS)	$MnAlCu_2$($L2_1$) [32]	$MnAlCu_2$ ($L2_1$)
C_{11}	147.51	158	137	138.26	140
C_{12}	122.08	117	141	116.56	123
C_{44}	99.25	108	107	103.02	105

The apparent instability of the SQS Al-Cu system complicates the computer-aided search for Gum-Metal-like materials. An AlCu BCC solid solution is known to exist at temperatures above 843 K[51], but finite temperature effects are beyond the scope of this paper. However, there is an extensive literature on β-stabilizers for Al-Cu. Lanzini *et al.*[52] found the order-disorder transformation in Al-Cu to be first-order. Fe, Mn, Ni, Sn, Be, Zn, and Cr are known to either maintain or lower the β transition temperature for an $Al_{0.25-y}Cu_{0.75-y}X_{2y}$ system [53]. Cr has been shown to help stabilize high-entropy alloys containing Al and Cu [54]. In addition, a BCC solid solution for Al-Cu-Cr exists at 873 K [55]. A BCC solid solution exists near $Al_{0.25}Cu_{0.75}$ at similar temperatures for Al-Cu-Zn systems [56].

Since $MnAlCu_2$ in the $L2_1$ structure also displays a high anisotropy (see Table I) the Al-Cu-Mn systems merit further consideration. Al-Cu-Mn systems are known SMAs.[39] At low Al compositions (less than 16 at.-% Al) the BCC phase can be stabilized at room temperature via quenching. The resulting alloy exhibits super-elasticity (7.5%), high ductility (15% elongation to fracture), and a yield strength of $250 - 500$ MPa [57]. Similar to Gum Metal, low Al content Al-Cu-Mn alloys show significant cold-workability (60 - 90 % rolling reduction before cracking). In another parallel, Al-Cu-Mn, as well as Cu-Zn-Al alloys exhibit Invar behavior [58]. It is still not clear if this Invar behavior found in Al-Cu-X systems is due to

the same mechanism as in Gum Metal. Al-Cu-X materials' Invar behavior appears to be a direct result of a martensitic transformation, while there exist contradictory observations for Gum Metal [14, 59]. Based on the analysis presented here and the experimental data, we hypothesize that severely cold-working a disordered Al-Cu-Mn alloy with the proper composition will generate an alloy with Gum-Metal-like properties.

In conclusion, a methodology for the computational discovery of Gum-Metal-like alloys is introduced. The method rests on the identification of a dislocation-based elastic anisotropy parameter that has been linked with the interesting behavior of Gum Metal. This parameter is then used in conjunction with data from the Materials Project to construct a structure map that allows identification of materials susceptible to Gum-Metal-like behavior, and several candidate alloys are identified. Though the identification of Gum Metals is the primary focus of the work, it is noted that the A_c structure maps may be useful for discovering and optimizing both SMAs and HEAs.

The authors acknowledge funding through the Materials Project Center funded by the Department of Energy Basic Energy Science grant No. EDCBEE.

---

* dcchrzan@berkeley.edu

[1] W. Xiong and G. B. Olson, MRS Bull. **40**, 1035 (2015).

[2] G. B. Olson and C. J. Kuehmann, Scr. Mater. **70**, 25 (2014).

[3] G. B. Olson and C. J. Kuehmann, Scr. Mater. **70**, 25 (2014).

[4] H. Bhadeshia, Scr. Mater. **70**, 12 (2014).

[5] M. L. Cohen and A. Y. Liu, Science (80-.). **245**, 841 (1989).

[6] A. Y. Liu and M. L. Cohen, Phys. Rev. B **41**, 10727 (1990).

[7] S. Veprek, Journal of Vacuum Science & Technology A: Vacuum, Surfaces, and Films **17**, 2401 (1999).

[8] S. Veprek, Journal of Vacuum Science & Technology A: Vacuum, Surfaces, and Films **31**, 050822_1 (2013).

[9] M. T. Yeung, R. Mohammadi, and R. B. Kaner, Annual Review of Materials Research **46**, 465 (2016).

[10] D. B. Miracle, J. D. Miller, O. N. Senkov, C. Woodward, M. D. Uchic, and J. Tiley, Entropy **16**, 494 (2014).

[11] M.-H. Tsai and J.-W. Yeh, Materials Research Letters **2**, 107 (2014).

[12] C. Jiang and B. P. Uberuaga, Phys. Rev. Lett. **116**, 105501 (2016).

[13] Z. Li, K. G. Pradeep, Y. Deng, D. Raabe, and C. C. Tasan, Nature **534**, 227 (2016).

[14] T. Saito, T. Furuta, J.-H. Hwang, S. Kuramoto, K. Nishino, N. Suzuki, R. Chen, A. Yamada, K. Ito, Y. Seno, T. Nonaka, H. Ikehata, N. Nagasako, C. Iwamoto, Y. Ikuhara, and T. Sakuma, Science **300**, 464 (2003).

[15] T. Li, J. W. Morris, N. Nagasako, S. Kuramoto, and D. C. Chrzan, Phys. Rev. Lett. **98**, 105503 (2007).

[16] E. Plancher, C. Tasan, S. Sandloebes, and D. Raabe, Scr. Mater. **68**, 805 (2013).

[17] M. J. Lai, C. C. Tasan, and D. Raabe, Acta Materialia **100**, 290 (2015).

[18] T. Furuta, S. Kuramoto, J. W. Morris, N. Nagasako, E. Withey, and D. C. Chrzan, Scr. Mater. **68** (2013), 10.1016/j.scriptamat.2013.01.027.

[19] N. Nagasako, R. Asahi, D. Isheim, D. N. Seidman, S. Kuramoto, and T. Furuta, Acta Mater. **105**, 347 (2016).

[20] C. Baker, Metal Science Journal **5**, 92 (1971).

[21] S. Kuramoto, N. Nagasako, T. Furuta, and Z. Horita, J. Alloys Compd. **577**, S147 (2013).

[22] H. Ikehata, N. Nagasako, T. Furuta, A. Fukumoto, K. Miwa, and T. Saito, Phys. Rev. B **70**, 1 (2004).

[23] S. Kuramoto, T. Furuta, N. Nagasako, and Z. Horita, Appl. Phys. Lett. **95**, 1 (2009).

[24] C. A. Sawyer, J. W. Morris, and D. C. Chrzan, Phys. Rev. B **87**, 134106 (2013).

[25] D. C. Chrzan, M. P. Sherburne, Y. Hanlumyuang, T. Li, and J. W. Morris, Phys. Rev. B **82**, 184202 (2010).

[26] M. Y. Gutkin, T. Ishizaki, S. Kuramoto, and I. A. Ovid'ko, Acta Mater. **54**, 2489 (2006).

[27] D. Roundy, C. R. Krenn, M. L. Cohen, and J. W. Morris, Philos. Mag. A **81**, 1725 (2001).

[28] W. Luo, D. Roundy, M. L. Cohen, and J. W. Morris, Phys. Rev. B **66**, 094110 (2002).

[29] N. Nagasako, M. Jahnátek, R. Asahi, and J. Hafner, Phys. Rev. B **81**, 94108 (2010).

[30] L. Qi and D. C. Chrzan, Phys. Rev. Lett. **112**, 1 (2014).

[31] A. Jain, S. P. Ong, G. Hautier, W. Chen, W. D. Richards, S. Dacek, S. Cholia, D. Gunter, D. Skinner, G. Ceder, et al., Apl Materials **1**, 011002 (2013).

[32] M. de Jong, W. Chen, T. Angsten, A. Jain, R. Notestine, A. Gamst, M. Sluiter, C. Krishna Ande, S. van der Zwaag, J. J. Plata, C. Toher, S. Curtarolo, G. Ceder, K. A. Persson, and M. Asta, Sci. Data **2**, 1 (2015).

[33] K. Hanson and J. W. Morris Jr, J. Appl. Phys. **46**, 2378 (1975).

[34] C. R. Krenn, D. Roundy, J. W. Morris, and M. L. Cohen, Mater. Sci. Eng. A **319**, 111 (2001).

[35] a. N. Stroh, Philos. Mag. **3**, 625 (1958).

[36] P. Lazar, M. Jahnátek, J. Hafner, N. Nagasako, R. Asahi, C. Blaas-Schenner, M. Stöhr, and R. Podloucky, Phys. Rev. B **84**, 054202 (2011).

[37] K. Otsuka and X. Ren, Mater. Sci. Eng. A **273-275**, 89 (1999).

[38] H. Y. Kim, S. Hashimoto, J. I. Kim, H. Hosoda, and S. Miyazaki, Mater. Trans. **45**, 2443 (2004).

[39] Y. Sutou, T. Omori, R. Kainuma, and K. Ishida, Mater. Sci. Technol. **24**, 896 (2008).

[40] K. Otsuka, K. Oda, Y. Ueno, M. Piao, T. Ueki, and H. Horikawa, Scripta metallurgica et materialia **29**, 1355 (1993).

[41] Y. Yamabe-Mitarai, R. Arockiakumar, A. Wadood, K. S. Suresh, T. Kitashima, T. Hara, M. Shimojo, W. Tasaki, M. Takahashi, S. Takahashi, and Others, Mater. Today Proc. **2**, S517 (2015).

[42] T. Duerig, J. Albrecht, D. Richter, and P. Fischer, Acta Metallurgica **30**, 2161 (1982).

[43] G. Kresse and J. Furthmüller, Phys. Rev. B **54**, 11169 (1996).

[44] G. Kresse and J. Hafner, Phys. Rev. B **47**, 558 (1993).

[45] J. P. Perdew, K. Burke, and M. Ernzerhof, Phys. Rev. Lett. **77**, 3865 (1996).

[46] M. Methfessel and A. T. Paxton, Phys. Rev. B **40**, 3616 (1989).

[47] A. Zunger, S.-H. Wei, L. G. Ferreira, and J. E. Bernard, Phys. Rev. Lett. **65**, 353 (1990).

[48] S.-H. Wei, L. G. Ferreira, J. E. Bernard, and A. Zunger, Phys. Rev. B **42**, 9622 (1990).

[49] A. van de Walle, P. Tiwary, M. de Jong, D. Olmsted, M. Asta, A. Dick, D. Shin, Y. Wang, L.-Q. Chen, and Z.-K. Liu, Calphad **42**, 13 (2013).

[50] M. de Jong, D. L. Olmsted, A. van de Walle, and M. Asta, Phys. Rev. B **86**, 224101 (2012).

[51] S.-W. Chen, Y.-Y. Chuang, Y. A. Chang, and M. G. Chu, Metall. Trans. A **22**, 2837 (1991).

[52] F. Lanzini, R. Romero, and M. L. Castro, Intermetallics **16**, 1090 (2008).

[53] "Asm alloy phase diagram database," http://mio.asminternational.org/apd/index.aspx.

[54] L. H. Wen, H. C. Kou, J. S. Li, H. Chang, X. Y. Xue, and L. Zhou, Intermetallics **17**, 266 (2009).

[55] A. P. Prevarskii and R. V. Skolozdra, Russian Metallurgy **1**, 137 (1972).

[56] G. Ghosh and H. J. V., Ternary Alloys **5**, 92 (1992).

[57] R. Kainuma, S. Takahashi, and K. Ishida, Metall. Mater. Trans. A **27** (1996).

[58] R. Kainuma, J. J. Wang, T. Omori, Y. Sutou, and K. Ishida, Appl. Phys. Lett. **80**, 4348 (2002).

[59] H. Y. Kim, L. Wei, S. Kobayashi, M. Tahara, and S. Miyazaki, Acta Mater. **61**, 4874 (2013).